Molecular basis of transport and regulation in the Na+/betaine symporter BetP

Ressl, Susanne; Terwisscha van Scheltinga, Anke C.; Vonrhein, Clemens; Ott, Vera; Ziegler, Christine

Published in:
Nature

DOI:
10.1038/nature07819

Publication date:
2009

ARTICLES

Molecular basis of transport and regulation in the Na^+/betaine symporter BetP

Susanne Ressl[1], Anke C. Terwisscha van Scheltinga[1], Clemens Vonrhein[2], Vera Ott[3] & Christine Ziegler[1]

Osmoregulated transporters sense intracellular osmotic pressure and respond to hyperosmotic stress by accumulation of osmolytes to restore normal hydration levels. Here we report the determination of the X-ray structure of a member of the family of betaine/choline/carnitine transporters, the Na^+-coupled symporter BetP from *Corynebacterium glutamicum*, which is a highly effective osmoregulated uptake system for glycine betaine. Glycine betaine is bound in a tryptophan box occluded from both sides of the membrane with aromatic side chains lining the transport pathway. BetP has the same overall fold as three unrelated Na^+-coupled symporters. Whereas these are crystallized in either the outward-facing or the inward-facing conformation, the BetP structure reveals a unique intermediate conformation in the Na^+-coupled transport cycle. The trimeric architecture of BetP and the break in three-fold symmetry by the osmosensing C-terminal helices suggest a regulatory mechanism of Na^+-coupled osmolyte transport to counteract osmotic stress.

Microorganisms must be able to adapt rapidly to extreme variations in salinity, temperature or osmolarity. To avoid dehydration or swelling, the cells adjust their intracellular solute pool[1]. Many organisms have developed similar strategies to counteract high osmolarity through the intracellular accumulation of osmolytes[2–4], which are often referred to as compatible solutes[1].

Osmolytes are highly polar, organic compounds that can accumulate in the cytosol to molar concentrations[4]. The osmolyte glycine betaine (*N*,*N*,*N*-trimethylglycine), often referred to simply as betaine, is widely used in osmoregulation by bacteria[5,6], archaea[7–9], fungi[10], plants[11] and animal cells[12–14]. Osmolytes promote protein stability through unfavourable interactions with the unfolded state[15], thus counteracting destabilizing agents such as urea, which is physiologically important in mammals[13,16]. Many microorganisms do not rely on the *de novo* synthesis of osmolytes[17,18], but instead use high-affinity transporters to import them from extracellular sources[6]. Osmolyte transporters are thus faced with the problem of binding a substrate that tends to be repelled by the protein surfaces[19].

The osmoregulated betaine transporter BetP of *C. glutamicum*[20] is a well-characterized member of the family of betaine/choline/carnitine transporters (BCCTs)[21], which contains a conserved tryptophan motif in transmembrane helix 8 (TM8). The transport of betaine by BetP is highly specific, and coupled to the symport of two Na^+ ions[22]. Betaine uptake is instantly activated by hyperosmotic stress, which causes an increase in cytoplasmic K^+ concentration sensed by the C-terminal domain of BetP[23–25].

We determined the structure of an N-terminally truncated and surface-engineered, but nevertheless active and osmoregulated, BetP mutant. The crystal structure shows BetP to be a trimer with three-fold non-crystallographic symmetry (NCS), whereas it is an asymmetric trimer in the membrane[24,25]. The transporter core consists of two tightly nested, structurally related inverted repeats of five transmembrane helices each. Its fold resembles that of the Na^+/alanine transporter $LeuT_{Aa}$ from *Aquifex aeolicus*[26], of the neurotransmitter/sodium symporter[27] (NSS) family, the Na^+/galactose transporter vSGLT from *Vibrio parahaemolyticus*[28], of the sodium/solute symporter[29] (SSS) family, and the benzyl hydantoin symporter Mhp1 from *Microbacterium liquefaciens*, of the nucleobase/cation symport 1 (ref. 30) family, which do not share any sequence homology with one another or with the BCCT family. Unlike the three other Na^+-coupled transporters, which represent an outward-facing ($LeuT_{Aa}$[26] and Mhp1[30]) or an inward-facing conformation (vSGLT[28]), the X-ray structure of BetP shows an occluded-intermediate, substrate-bound state. Comparison of these structures provides new insights into conformational changes during the transport cycle of Na^+-coupled symporters. Furthermore, different interactions between neighbouring monomers in the BetP trimer suggest a regulatory mechanism in response to osmotic stress.

Transporter structure

Apart from the extended C-terminal α-helix, the BetP monomer has a nearly cylindrical shape (Fig. 1a). It contains twelve transmembrane α-helices (Fig. 1b) and a curved α-helix (H7, helix 7) at the periplasmic membrane surface. Three helices at the perimeter of the monomer (TM1, TM11 and TM6) run almost perpendicular to the membrane, whereas TM5, TM10 and TM12 are substantially tilted by about ~40°.

TM3 has a locally unwound segment, approximately halfway across the membrane, that divides it into intracellular (TM3i) and extracellular (TM3e) parts. TM4 and TM5 are connected on the cytoplasmic side by loop 4, which includes an internal 3_{10} helix (IH1). TM9 and TM10 are connected on the periplasmic side by loop 9, which contains a short external α-helix (EH2). TM3, TM4, TM8 and TM9 form an iris-shaped, four-helix bundle with a prominent non-protein density in its centre roughly halfway along TM4 and TM8, adjacent to the unwound region separating TM3i and TM3e. This density was identified by its shape and by structural-substrate coordination homology[31] as betaine (Fig. 2 and Supplementary Fig. 1a).

[1]Max Planck Institute of Biophysics, Department of Structural Biology, 60438 Frankfurt am Main, Germany. [2]Global Phasing Ltd, Sheraton House, Castle Park, Cambridge CB3 0AX, UK. [3]Institut für Biochemie, Universität zu Köln, 50937 Köln, Germany.

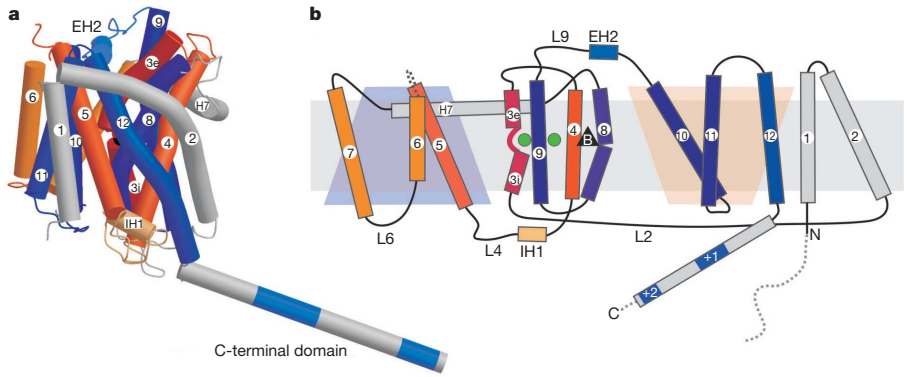

Figure 1 | Structure of an N-terminally truncated, surface-engineered BetP mutant. a, Side view of monomer A. Colouring and numbering of the helices (cylinders) are as in Fig. 1b. Repeat 1 (TM3–TM7) is orange, with colour intensity decreasing from the N terminus to the C terminus. The topologically related repeat 2 (TM8–TM12) is coloured blue in a similar way. TM1, TM2, helix 7 and the C-terminal domains are grey. The clusters of positive charges in the C-terminal helix are indicated in blue. **b**, Inverted repeats in the BetP topology. The substrate is represented as a black triangle and the sodium ions are green. Unresolved residues are indicated by a dotted line. Important loops are indicated as L2, L4, L6 and L9.

The ten C-terminal transmembrane helices contain an internal structural repeat, which is not evident in the amino-acid sequence of BetP, forming the core of the transporter. The structural repeat relates TM3–TM7 to TM8–TM12 by a pseudo-two-fold axis in the plane of the membrane (Fig. 1b). The V-shaped helix pair TM3–TM4 is closely nested with the inverted V-shaped pair TM8–TM9, forming the four-helix bundle, which is surrounded by TM5–TM7 and TM10–TM12 serving as a scaffold. The long, curved helix 7 and TM2 enclose the transporter core like a stabilizing belt.

The significant resemblance in overall architecture of the inverted structural repeats in the different Na^+-coupled symporters BetP, $LeuT_{Aa}$[26], vSGLT[28] and Mhp1[30] is not reflected in sequence similarity. Furthermore, the similar fold provides new insights in the relation of bacterial BCCTs and eukaryotic GABA (γ-aminobutyric acid)/osmolyte transporters from the NSS family found in kidney[32] and in brain[33]. Most likely, they have a common ten-transmembrane-helix ancestor that evolved by gene duplication and harboured the inverted repeat, which then diverged in the course of evolution as dictated by environmental conditions[34].

Substrate pathway

Side chains from TM4 and TM8 contribute to the betaine-binding site (Fig. 2). As in betaine-specific binding proteins[31,35,36], the quaternary ammonium group is enclosed in an aromatic environment by cation–π and van der Waals interactions. In BetP, indole groups of Trp 189 and Trp 194 (TM4) and Trp 374 (TM8) form the aromatic box. The indole groups of Trp 194 and Trp 374 are almost parallel, whereas Trp 189 is approximately perpendicular to both and forms a lid on the periplasmic side. The side chain of Tyr 197 makes up the fourth side of the aromatic box. Trp 194 is conserved in the BCCT family, but Trp 189, Tyr 197 and Trp 374 are only conserved in transporters of quaternary ammonium substrates, such as choline and carnitine (Supplementary Fig. 2). Replacement of Trp 189, Trp 194 and Tyr 197 in TM4 resulted in significantly reduced betaine uptake rates. Mutation of Trp 374 in TM8 leaves the transport rate unaffected (Supplementary Fig. 3), suggesting that the substrate is still accommodated, probably at a changed position, in the modified binding pocket. Removal of Trp 362, which pointed out of the substrate pathway into the periplasm, resulted in reduced activity (Supplementary Fig. 3), suggesting a role in substrate sequestration. Mutation of Trp 377 below the substrate-binding pocket inactivates BetP, but mutation of Trp 366 and Trp 371 does not affect activity (Supplementary Fig. 3). We suggest that Trp 377 may act as an additional binding site during conformational changes in the transport cycle.

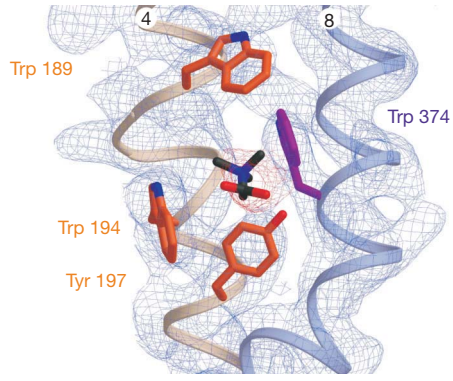

Figure 2 | The betaine-binding site. $2F_o - F_c$ map, contoured at 1σ, showing density for betaine (red) and the densities for TM4 (light brown) and TM8 (light blue) in blue. F_o and F_c are the observed and calculated structure functions, respectively. Side chains defining the tryptophan box of the betaine-binding motif are Trp 189, Trp 194, Trp 374 and Tyr 197.

In BetP and other members of the BCCT family (Supplementary Fig. 2), a total of 23 conserved aromatic side chains line the substrate pathway including the tryptophan box in the four-helix bundle (Supplementary Fig. 1b), raising the question of whether such an excessive supply is needed. According to the widely accepted alternating-access model of membrane transport[37], the interaction surface of the substrate and transporter need only extend to the central binding site that is switching accessibility from one side of the membrane to the other during the transport cycle. Usually, osmolytes act as co-solvents and are excluded from the first hydration shell of proteins by repulsive interaction with the protein backbone[38]. Coating the binding site with aromatic side chains would solve this problem, by providing a surface that would, according to Tanford's transfer model[39], minimally repel osmolytes[31,35,36,40].

Functional studies[22] have shown that two Na^+ ions are required to energize betaine transport in BetP, which has a Michaelis constant (K_m) for Na^+ of 39 mM (ref. 23). On the basis of the structural alignment of BetP on the $LeuT_{Aa}$[26] structure, we propose two potential Na^+ binding sites (Fig. 3a and Supplementary Fig. 4). Sodium binding in the active, osmoregulated BetP mutant used for structure determination (Supplementary Fig. 5) seems to be facilitated by main chain interactions in the flexible, glycine-rich stretch of TM3 with one Na^+ ion (Na1) coordinated by the carboxyl group of betaine, the carbonyl oxygen of Met 150 in the unwound region of TM3 and the carbonyl oxygen of Ala 148 in TM3i (Fig. 3a and Supplementary Fig. 4). The second Na^+ ion (Na2) is located in the bend between TM3e and TM3i. The carbonyl oxygen of Ala 147 in TM3i and the side chains of Ser 306 and Met 310 in TM7 coordinate Na2. Thr 467 and Ser 468 in TM10 are suggested to be additional ligands of Na1 and Na2 with an interaction probably mediated through water molecules.

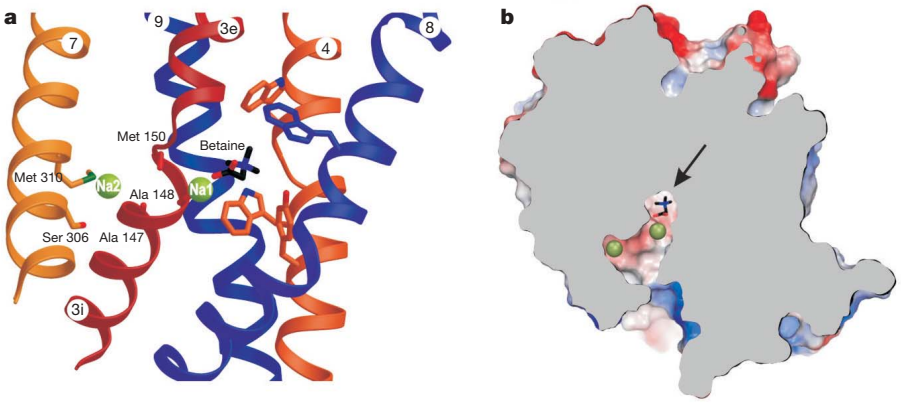

Figure 3 | The proposed sodium binding in BetP. **a**, Proposed Na^+ ion positions in BetP. Na1 is coordinated by the carboxyl group of betaine and residues in TM3i. Na2 is coordinated by residues in TM3i and TM7. **b**, Accessibility of the two Na^+ ion positions and betaine (arrow) from the cytoplasm in a section through the protein volume.

Ser 468 is conserved in the BCCT family, as are the corresponding Ser 355 in the NSS family and Ser 364 or Ser 365 in the SSS family. However, the glycines flanking Met 150 in the stretch of TM3 appear only to be conserved in transporters exhibiting a 2:1 Na^+:substrate stoichiometry (Supplementary Fig. 6). In the BCCT family, high-affinity betaine transporters (Supplementary Fig. 2) exclusively contain the conserved GxGxG motif in the segment of TM3, suggesting that BetP's specificity to betaine is related to the structure of the unwound segment upon binding of Na1.

The substrate pathway and the potential positions of the Na^+ ions are blocked from the periplasm in the BetP structure, but a narrow funnel between TM3i, TM7, TM8 and TM10 links the putative Na sites to the cytoplasm (Fig. 3b). The funnel has an elliptical constriction defined by Ala 147 (TM3), Ile 302 and Ser 306 (TM7), Phe 380 and Phe 384 (TM8) and Ser 471 (TM10), with a major axis of ~4.5 Å and a minor axis of ~2 Å. For steric reasons and owing to the limited side-chain size of the residues involved in the constriction, the opening of the funnel will require a rearrangement of the polypeptide backbone, that is, a considerable conformational change (Fig. 4b). By also taking into account the structural symmetry of the two repeats (Supplementary Table 2), we conclude that BetP displays a unique intermediate state in the Na^+-coupled transport cycle, which

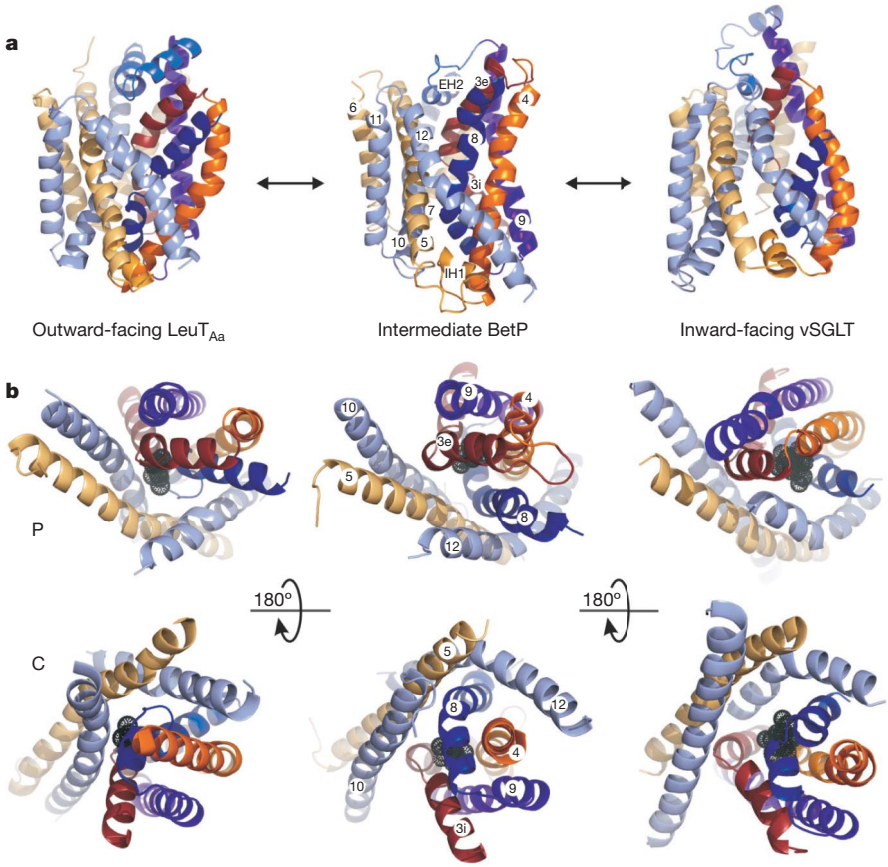

Figure 4 | Conformational changes in Na^+-coupled transport. **a**, Side view of the four-helix bundles (TM3, TM4, TM8 and TM9) and the surrounding stabilizing scaffold (TM5–TM7 and TM10–TM12) in $LeuT_{Aa}$, BetP and vSGLT. Numbering of the helices is as in BetP. **b**, Top view of the four-helix bundles and a part of the scaffold (TM5, TM10 and TM12) from the periplasm (P) and the cytoplasm (C). Grey spheres indicate the bound substrate.

differs significantly from the occluded periplasmically or cytoplasmically open states described before[26,28,30].

Transport mechanism

Although the available transporter structures[26,28,30,41] support the alternating-access model of membrane transport[37], so far none of them show the same transporter in more than one conformation. The central question of how the different conformations interconvert to bring about membrane transport has thus remained unanswered. BetP, $LeuT_{Aa}$[26], Mhp1[30] and vSGLT[28] contain similar topologically inverted repeats that can be superimposed unambiguously (Supplementary Table 2). Structural differences among these repeats contribute to the asymmetric architecture of the outward- and inward-facing conformations of $LeuT_{Aa}$/Mhp1 and vSGLT, respectively (Fig. 4a)[42].

Previous modelling studies[42] could only exploit this asymmetry and described the change from the outward-facing conformation to the inward-facing conformation as a switching of the conformation of the two repeats. However, the occluded-intermediate state of BetP has a symmetrical architecture (Fig. 4a and Supplementary Table 2), which allows the conformational changes to be described in more detail through discussion of the periplasmically open, occluded-intermediate and cytoplasmically open conformations observed in the different transporters in terms of a single, unified transport mechanism.

The striking resemblance of the periplasmically open conformation in $LeuT_{Aa}$ and Mhp1 suggests that the conformations observed in the different transporters are applicable to each other. Also in this context, structural alignments show a number of structurally related glycines in BetP, $LeuT_{Aa}$, vSGLT and Mhp1 in both repeats conserved in their respective families. Recent hydropathy-profile alignments[43] revealed a characteristic clustering of hydrophobic residues in transmembrane helices in transporters of the unrelated NSS, SSS and amino acid/polyamine/organocation families, confirming their similar transporter core structures.

On changing from the outward-facing conformation ($LeuT_{Aa}$) over an intermediate state (BetP) to the inward-facing conformation (vSGLT; Fig. 4b), a concerted, iris-like movement occurs in the four-helix bundle. The periplasmic halves of TM3, TM4 and TM9 (BetP numbering) undergo an anticlockwise rotation occluding the substrate-binding site on the periplasmic side (Fig. 4b). The concomitant movement of TM8 might be influenced by the different sizes and natures of the substrates in the three transporters. The rotation of the cytoplasmic half of the four-helix bundle moves it out of the centre of the transporter. In the scaffold surrounding the four-helix bundle, TM10 straightens and TM5 and TM12 approach TM3 and TM8 on the periplasmic side. On the cytoplasmic side, they move away from the four-helix bundle, opening a route to the substrate-binding site between TM8 and TM12. The conformational changes associated with transport can thus be described in terms of concerted movements of the four-helix bundle and the surrounding scaffold. The pivot points of these movements are located near the substrate- and ion-binding sites, close to the structurally conserved glycines as in the GxGxG motif in the stretch of TM3 and Gly 301 in loop 6 (Supplementary Fig. 6). Ile 302 and Ser 306, both of which are involved in the occlusion of the substrate from the cytoplasm, follow Gly 301. Notably, mutation of Gly 301 renders BetP inactive (Supplementary Fig. 3). Therefore, this glycine might be important for the flexibility of loop 6 and, thus, for opening this pathway to the cytoplasm.

Mutagenesis studies of the $LeuT_{Aa}$ homologue SERT reveal conformational changes during transport in the loop connecting the four-helix bundle with the C-terminal part of the scaffold[44,45]. A comparison of the three structures indicates a major shift in the N-terminal part of this loop 9, moving out of the periplasmic vestibule in the transition to the inward-facing conformation (Fig. 4a).

In the occluded state of the BetP structure, helices adopt intermediate positions between the outward- and inward-facing conformations of $LeuT_{Aa}$ and vSGLT. Therefore, conformational changes during inward transport do not seem to be a mere switching motion between the two low-energy open states, as predicted by the alternating-access model, but seem to involve an additional low-energy intermediate state resulting from the concerted movement of transmembrane helices around the coupling ion-binding sites.

Trimer architecture

The three monomers labelled A, B, and C in Fig. 5a are related by a three-fold NCS axis, which run perpendicular to the membrane. The trimer has a central conical cavity (Fig. 5c, d) and is lined by 3×4 aromatic side chains (Supplementary Fig. 7). Other than in this hydrophobic cavity, the cytoplasmic surface is positively charged, whereas the periplasmic surface is negatively charged (Fig. 5d). The hydrophobic cavity is filled with non-protein density, most likely detergent or lipid. The segment of helix 7 that faces the periplasm is rich in leucines and asparagines. Therefore, it shows characteristics of a non-specific lipid interaction site[46] and may bind lipid in the central cavity to stabilize the trimer. There are deep clefts between the monomers, which are accessible from the membrane. In the membrane these would be filled with lipids, allowing the monomers in the trimer to move.

Interactions between monomers involve the C-terminal helix and the amphipathic helix 7. Helix 7 makes contact with TM2, TM3, TM9 and helix 7 of the other two monomers, and the C-terminal helix interacts with loop 2 and the C termini of the other monomers. The BetP C terminus contains two clusters of positively charged residues, from Arg 558 to Arg 568 and from Lys 581 to Lys 587 (Fig. 1a). In the BetP structure, the C-terminal helices are all differently oriented and do not obey NCS (Fig. 5b); monomer A is resolved to Arg 589, monomer B to Arg 558 and monomer C to Arg 568. The second cluster is only resolved in the C terminus of monomer A, it mediates the main crystal contacts between trimers (Supplementary Fig. 8), which contribute to the break in NCS. However, other breaks of NCS are clearly not due to crystal contacts. Arg 568 residues of monomers A and C form a salt bridge to Glu 552 of the adjacent monomer. This interaction is not found for Arg 568 of monomer B (Fig. 6).

Regulation

Alanine and proline scanning of the C-terminal helix indicate that arginines in both clusters are important for regulation[47], which is lost upon C-terminal truncation at Tyr 550[24]. Peptide-array analysis[47] has implicated strong interactions of positively charged C-terminal domains with the negatively charged N-terminal domain. N-terminal truncation resulted in activation at higher osmolarity in *C. glutamicum* and in *Escherichia coli* polar lipid proteoliposomes (Supplementary Fig. 5), indicating that the interaction of C and N termini has an important role in regulation. When not constrained by crystal contacts, the C-terminal helix appears to have some freedom to move in a plane parallel to the membrane surface. In the BetP structure, the C terminus of monomer C points towards TM1 of monomer B, suggesting a possible interaction with the N-terminal domain, whereas the C terminus of monomer B is oriented towards TM6, suggesting to a potential interaction site with residues in loop 4 and loop 8.

The structure of BetP also reveals an important role for loop 2, which was observed by peptide-array analysis[47] to some extent. In a supposed outward-facing conformation of BetP (Fig. 4a), loop 2 would block the cytoplasmic funnel for the Na^+ ions and the substrate. Loop 2 contains the three negatively charged residues: Asp 131, Glu 132 and Glu 135. Double mutation at Asp 131 and Glu 132 prevents expression of the *betP* gene and mutation at Glu 135 reduces transport activity (Supplementary Fig. 3). Asp 131 interacts by means of a salt bridge with Arg 558 located in the C-terminal helix of the adjacent monomer, and Glu 132 with Arg 390 in loop 8, which connects TM8 and TM9 in the four-helix bundle (Fig. 6). Loop 8 contains an additional positively charged patch of Arg 387 and Arg 392, and

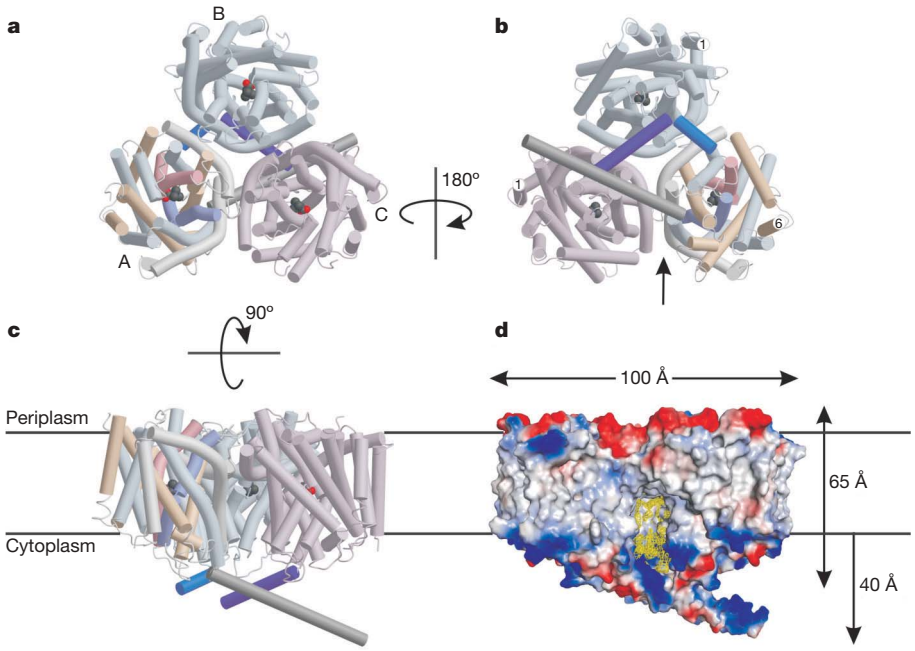

Figure 5 | Trimer architecture of BetP. a, **b**, The BetP trimer as seen from the periplasmic (**a**) and cytoplasmic (**b**) sides of the membrane. Monomers A (helices coloured as in Fig. 1, in a lighter tint), B (blue) and C (pink) are related by three-fold NCS with the exception of their C-terminal helices (darker colours). In monomers A and C in **b**, the C termini face the N termini of monomers C and B, respectively, whereas in monomer B, the C terminus points towards TM6 in monomer A. Monomers are separated by a cleft (arrow). **c**, View into the cleft between monomers A and C. The BetP trimer protrudes from the periplasmic membrane surface by about 10 Å. On the cytoplasmic side, the α-helical C-terminal domain of monomer A extends ~40 Å into the cell. **d**, Surface representation of the trimer oriented as in **c**. The electrostatic surface is coloured red (negative) to blue (positive). The $F_o - F_c$ non-protein density (2σ contour level) in the hydrophobic cavity (~37 Å in height and ~30 Å in diameter) is shown in yellow. The boundaries of the lipid bilayer are indicated in **c** and **d**.

transport activity is sensitive to mutation of both arginines (Supplementary Fig. 3).

Changes in orientation of the C-terminal helix would affect the orientation of Asp 131 and, in turn, Glu 132 and hence the conformation of loop 8, and could thus regulate the transport cycle by ionic interactions. In proteoliposomes, activation of BetP in response to osmotic stress seems to be specifically triggered by high internal K^+ concentration, although the activation optimum of 220 mM (refs 23, 48) is high for a specific K^+-binding region. In addition, the cation specificity depends on the membrane composition indicating concomitant or competing stimuli in osmoregulation. A direct interaction of the BetP C terminus with charged lipids in the membrane as observed by surface plasmon resonance[47] could influence the accessibility of a potential regulatory K^+-binding region. We suggest that the cation specificity most likely depends on the orientations of the C-terminal domains reflecting functionally different conformations in the activation cycle. Regulation of transport is thus a collective effect of the interactions between the three BetP monomers. Therefore, lipids in the clefts between the monomers or in the hydrophobic cavity in the centre of the trimer might affect the orientation of the C-terminal helices as well. We conclude that each monomer in the trimer activates its neighbour, taking advantage of the oligomeric architecture of BetP.

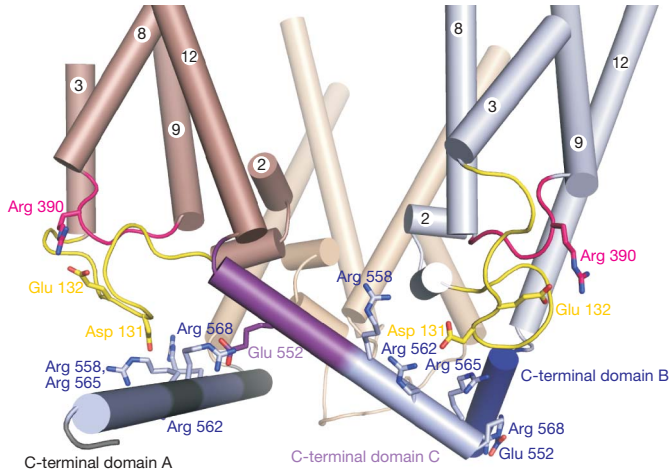

Figure 6 | Regulatory interactions mediated by the C-terminal domains. Ionic interactions of the C-terminal domains and the involved helices of monomer A (grey), monomer B (blue) and monomer C (brown-purple) with loop 2 (yellow) and loop 8 (red) on the cytoplasmic side. The two positively charged clusters in each domain are shown in light blue. Residues forming salt bridges are shown in stick representation and labelled separately.

METHODS SUMMARY

The construct of BetPΔN29EEE44/45/46AAA ($BetP\Delta N29_{Se}$) with an N-terminal StrepII tag in a IBA7 vector was used to express selenium-labelled protein in *E. coli* BL21 RIL-X cells at 37 °C, using SelenoMet media (Molecular Dimensions) containing 40 mg l^{-1} L-selenomethionine. The protein was solubilized from isolated membranes in 2.5% (w/v) β-dodecyl-maltoside and purified by affinity and size-exclusion chromatography. $BetP\Delta N29_{Se}$ crystals were grown by vapour diffusion at 18 °C by mixing a 1:1 volume of protein (~9 mg ml^{-1}) and reservoir solution containing 100 mM Na_3citrate (pH 5.55), 23% PEG 400 and 100 mM NaCl. A single-anomalous-dispersion diffraction data set to 3.3 Å was used to obtain phases from the selenium anomalous signal. The data were corrected for their strong anisotropy, and the resulting electron density was *B*-factor sharpened and averaged using the three-fold NCS operators. This resulted in an interpretable map, and the automatically built partial model was completed manually. The structure was refined to a final reliability factor $R_{work} = \sum||F_o| - |F_c||/\sum|F_o|$ of 25.6% and an R_{free} value (calculated for 5% of the data that were excluded from the refinement) of 26.5%. Uptake of [^{14}C]glycine betaine by BetP and mutants was measured in *E. coli* MKH13, in *C. glutamicum* DHPF cells and in *E. coli* polar lipid proteoliposomes as described[23,24,48]. The osmolality was adjusted to 800 mosmol kg^{-1} by addition of sorbitol. Substrate uptake in cells or proteoliposomes was initiated by adding [^{14}C]glycine betaine (0.1 mCi ml^{-1}) at a final concentration of 100 or 200 mM and measured as described[48].

Full Methods and any associated references are available in the online version of the paper at www.nature.com/nature.

Received 18 July 2008; accepted 21 January 2009.

1. Burg, M. B. Molecular basis of osmotic regulation. *Am. J. Physiol.* **268,** F983–F996 (1995).
2. Kinne, R. K. The role of organic osmolytes in osmoregulation: from bacteria to mammals. *J. Exp. Zool.* **265,** 346–355 (1993).
3. Yancey, P. H. Organic osmolytes as compatible, metabolic and counteracting cytoprotectants in high osmolarity and other stresses. *J. Exp. Biol.* **208,** 2819–2830 (2005).
4. Burg, M. B. & Ferraris, J. D. Intracellular organic osmolytes: function and regulation. *J. Biol. Chem.* **283,** 7309–7313 (2008).
5. Wood, J. M. *et al.* Osmosensing and osmoregulatory compatible solute accumulation by bacteria. *Comp. Biochem. Physiol. A* **130,** 437–460 (2001).
6. Wood, J. M. Bacterial osmosensing transporters. *Methods Enzymol.* **428,** 77–107 (2007).
7. da Costa, M. S., Santos, H. & Galinski, E. A. An overview of the role and diversity of compatible solutes in Bacteria and Archaea. *Adv. Biochem. Eng. Biotechnol.* **61,** 117–153 (1998).
8. Roberts, M. F. Osmoadaptation and osmoregulation in archaea. *Front. Biosci.* **5,** D796–D812 (2000).
9. Pflüger, K. & Müller, V. Transport of compatible solutes in extremophiles. *J. Bioenerg. Biomembr.* **36,** 17–24 (2004).
10. Blomberg, A. Osmoresponsive proteins and functional assessment strategies in *Saccharomyces cerevisiae*. *Electrophoresis* **18,** 1429–1440 (1997).
11. Tuteja, N. Mechanisms of high salinity tolerance in plants. *Methods Enzymol.* **428,** 419–438 (2007).
12. Beck, F. X. & Neuhofer, W. Response of renal medullary cells to osmotic stress. *Contrib. Nephrol.* **148,** 21–34 (2005).
13. Lang, F. Mechanisms and significance of cell volume regulation. *J. Am. Coll. Nutr.* **26,** 613S–623S (2007).
14. Lim, C. H., Bot, A. G., de Jonge, H. R. & Tilly, B. C. Osmosignaling and volume regulation in intestinal epithelial cells. *Methods Enzymol.* **428,** 325–342 (2007).
15. Rösgen, J. Molecular basis of osmolyte effects on protein and metabolites. *Methods Enzymol.* **428,** 459–486 (2007).
16. Garcia-Perez, A. & Burg, M. B. Importance of organic osmolytes for osmoregulation by renal medullary cells. *Hypertension* **16,** 595–602 (1990).
17. Kempf, B. & Bremer, E. Uptake and synthesis of compatible solutes as microbial stress responses to high-osmolality environments. *Arch. Microbiol.* **170,** 319–330 (1998).
18. Empadinhas, N. & da Costa, M. S. Diversity and biosynthesis of compatible solutes in hyper/thermophiles. *Int. Microbiol.* **9,** 199–206 (2006).
19. Athawale, M. V., Dordick, J. S. & Garde, S. Osmolyte trimethylamine-N-oxide does not affect the strength of hydrophobic interactions: origin of osmolyte compatibility. *Biophys. J.* **89,** 858–866 (2005).
20. Peter, H., Burkovski, A. & Krämer, R. Isolation, characterization, and expression of the *Corynebacterium glutamicum* betP gene, encoding the transport system for the compatible solute betaine. *J. Bacteriol.* **178,** 5229–5234 (1996).
21. Kappes, R. M., Kempf, B. & Bremer, E. Three transport systems for the osmoprotectant betaine operate in *Bacillus subtilis*: characterization of OpuD. *J. Bacteriol.* **178,** 5071–5079 (1996).
22. Farwick, M., Siewe, R. M. & Krämer, R. Betaine uptake after hyperosmotic shift in *Corynebacterium glutamicum*. *J. Bacteriol.* **177,** 4690–4695 (1995).
23. Schiller, D., Krämer, R. & Morbach, S. Cation specificity of osmosensing by the betaine carrier BetP of *Corynebacterium glutamicum*. *FEBS Lett.* **563,** 108–112 (2004).
24. Peter, H., Burkovski, A. & Krämer, R. Osmo-sensing by N- and C-terminal extensions of the betaine uptake system BetP of *Corynebacterium glutamicum*. *J. Biol. Chem.* **273,** 2567–2574 (1998).
25. Ziegler, C. *et al.* Projection structure and oligomeric state of the osmoregulated sodium/betaine symporter BetP of *Corynebacterium glutamicum*. *J. Mol. Biol.* **337,** 1137–1147 (2004).
26. Yamashita, A., Singh, S. K., Kawate, T., Jin, Y. & Gouaux, E. Crystal structure of a bacterial homologue of Na^+/Cl^--dependent neurotransmitter transporters. *Nature* **437,** 215–223 (2005).
27. Chang, A. B., Lin, R., Studley, W. K., Tran, C. V. & Saier, M. H. Jr. Phylogeny as a guide to structure and function of membrane transport proteins. *Mol. Membr. Biol.* **21,** 171–181 (2004).
28. Faham, S. *et al.* The crystal structure of a sodium galactose transporter reveals mechanistic insights into Na^+/sugar symport. *Science* **321,** 810–814 (2008).
29. Saier, M. H. J. Families of transmembrane sugar transport proteins. *Mol. Microbiol.* **35,** 699–710 (2000).
30. Weyand, S. *et al.* Structure and molecular mechanism of a nucleobase-cation-symport-1 family transporter. *Science* **322,** 709–713 (2008).
31. Schiefner, A. *et al.* Cation-π interactions as determinants for binding of the compatible solutes betaine and proline betaine by the periplasmic ligand-binding protein ProX from *Escherichia coli*. *J. Biol. Chem.* **279,** 5588–5596 (2004).
32. Kempson, S. A. & Montrose, M. H. Osmotic regulation of renal betaine transport: transcription and beyond. *Pflugers Arch.* **449,** 227–234 (2004).
33. Borden, L. A. GABA transporter heterogeneity: pharmacology and cellular localization. *Neurochem. Int.* **29,** 335–356 (1996).
34. Rapp, M. G. E., Seppälä, S. & von Heijne, G. Identification and evolution of dual-topology membrane proteins. *Nature Struct. Mol. Biol.* **13,** 112–116 (2006).
35. Schiefner, A., Holtmann, G., Diederichs, K., Welte, W. & Bremer, E. Structural basis for the binding of compatible solutes by ProX from the hyperthermophilic archaeon *Archaeoglobus fulgidus*. *J. Biol. Chem.* **279,** 48270–48281 (2004).
36. Horn, C. *et al.* Molecular determinants for substrate specificity of the ligand-binding protein OpuAC from *Bacillus subtilis* for the compatible solutes betaine and proline betaine. *J. Mol. Biol.* **357,** 592–606 (2006).
37. Jardetzky, O. Simple allosteric model for membrane pumps. *Nature* **211,** 969–970 (1966).
38. Bolen, D. W. & Rose, G. D. Structure and energetics of the hydrogen-bonded backbone in protein folding. *Annu. Rev. Biochem.* **77,** 339–362 (2008).
39. Tanford, C. Protein denaturation. C. Theoretical models for the mechanism of denaturation. *Adv. Protein Chem.* **24,** 1–95 (1970).
40. Kuhlmann, S. I., Terwisscha van Scheltinga, A. C., Bienert, R., Kunte, H. J. & Ziegler, C. Osmoregulated transport of compatible solutes in the halophilic bacterium *Halomonas elongata*: 1.55 Å high-resolution structure of the periplasmic ectoine-binding protein from TRAP-transporter TeaABC. *Biochemistry* **47,** 9475–9485 (2008).
41. Yernool, D., Boudker, O., Jin, Y. & Gouaux, E. Structure of a glutamate transporter homologue from *Pyrococcus horikoshii*. *Nature* **431,** 811–818 (2004).
42. Forrest, L. R. *et al.* Mechanism for alternating access in neurotransmitter transporters. *Proc. Natl Acad. Sci. USA* **105,** 10338–10343 (2008).
43. Lolkema, J. S. & Slotboom, D.-J. The major amino acid transporter superfamily has a similar core structure as Na^+-galactose and Na^+-leucine transporters. *Mol. Membr. Biol.* **25,** 567–570 (2008).
44. Smicun, Y., Campbell, S. D., Chen, M. A., Gu, H. & Rudnick, G. The role of external loop regions in serotonin transport. Loop scanning mutagenesis of the serotonin transporter external domain. *J. Biol. Chem.* **274,** 36058–36064 (1999).
45. Stephan, M. M., Chen, M. A., Penado, K. M. & Rudnick, G. An extracellular loop region of the serotonin transporter may be involved in the translocation mechanism. *Biochemistry* **36,** 1322–1330 (1997).
46. Palsdottir, H. & Hunte, C. Lipids in membrane protein structures. *Biochim. Biophys. Acta* **1666,** 2–18 (2004).
47. Ott, V., Koch, J., Späte, K., Morbach, S. & Krämer, R. Regulatory properties and interaction of the C- and N-terminal domains of BetP, an osmoregulated betaine transporter from *Corynebacterium glutamicum*. *Biochemistry* **47,** 12208–12218 (2008).
48. Schiller, D., Rübenhagen, R., Krämer, R. & Morbach, S. The C-terminal domain of the betaine carrier BetP of *Corynebacterium glutamicum* is directly involved in sensing K^+ as an osmotic stimulus. *Biochemistry* **43,** 5583–5591 (2004).

Supplementary Information is linked to the online version of the paper at www.nature.com/nature.

Acknowledgements The authors thank W. Kühlbrandt and R. Krämer for support and comments on the manuscript; J. Standfuß for contributions in the early stages of the project; Ö. Yildiz, T. Barros and R. Wouts for computational support; S. Schulze, S. Morbach, S. Nicklisch and L. Forrest for discussions; J. Hakulinen and J. Carrera for cloning, C. Perez for the reconstitution and freeze fracture experiments; and H. Volk for help with the figures. Special thanks are due to E. Pohl and the X10SA beamline staff at the Swiss Light Source, as well as the European Synchrotron Radiation Facility. This work is supported by the German Research Foundation, Collaborative Research Centre 807 'Transport and Communication across Biological Membranes'.

Author Information The coordinates for the structure reported in this work have been deposited in the Protein Data Bank under accession number 2W8A. Reprints and permissions information is available at www.nature.com/reprints. Correspondence and requests for materials should be addressed to C.Z. (christine.ziegler@mpibp-frankfurt.mpg.de).

METHODS

Purification and crystallization. The plasmid IBA7*betPΔN29EEE44/45/46AAA* containing an N-terminal StrepII tag was constructed as described[23]. For selenomethionine labelling, the plasmid was transformed into *E. coli* BL21 RIL-X cells (Stratagene). The cells were cultured in SelenoMet media (Molecular Dimensions) containing 40 mg l^{-1} L-selenomethionine and BetP*ΔN29EEE44/45/46AAA* (BetPΔN29$_{Se}$) was produced after induction at an absorbance at 600 nm ($A_{600\,nm}$) of 0.7 with 200 μg l^{-1} anhydrotetracycline for 6 h at 37 °C. Membranes were isolated from disrupted cells and solubilized in 2.5% (w/v) β-dodecyl-maltoside (DDM, Glycon) for 40 min on ice under an N_2 stream. To minimize oxidation, 5 mM dithiothreitol and 0.5 mM EDTA were added at all subsequent steps. BetPΔN29$_{Se}$ was eluted with 5 mM desthiobiotin from the Streptactin resin (IBA GmbH) affinity column in buffer containing 25 mM Tris-HCl (pH 7.5), 200 mM NaCl, 8.7% glycerol and 0.6% Cymal-5. The protein was loaded onto a Superose 6 (GE Healthcare) size-exclusion column equilibrated with 20 mM Tris-HCl (pH 7.5), 200 mM NaCl and 0.6% Cymal-5. Purified protein was concentrated at 4 °C to ~10 mg ml^{-1} at 3,000 g in a Vivaspin tube (Vivascience) with a 100,000-molecular-weight cut-off.

BetPΔN29 and BetPΔN29$_{Se}$ crystallized reproducibly with a reservoir solution of 100 mM Na_3citrate (pH 5.3–5.6), 14–24% PEG 400 and 100–150 mM NaCl. Crystals typically grew at 18 °C upon mixing the protein solution in 1:1 or 1:2 ratio with the reservoir solution. Addition of glycine betaine resulted in poor crystal growth, but sufficient amounts of the substrate were present in the SelenoMet medium to bind to BetP, and to remain bound during purification and crystallization. A concentration of 100 mM NaCl was necessary for well-diffracting crystals. Other salts did not produce crystals. Crystals were cryoprotected with a mixture of Paratone N and paraffin oil before freezing in liquid nitrogen. The crystals belong to orthorhombic space group $P2_12_12_1$ with cell dimensions $a = 118.1$ Å, $b = 129.4$ Å and $c = 182.9$ Å, and diffract to 2.7 Å along b^* and 3.8 Å along a^* and c^* (Supplementary Table 1).

Structure determination. X-ray diffraction data were collected on a mar225 charge-coupled device detector at the Max Planck beamline X10SA (PXII) at the Swiss Light Source in Villingen, Switzerland, processed with XDS[49] and scaled with SCALA[50]. Phases were obtained by single anomalous dispersion from a data set (Supplementary Table 1) of a BetPΔN29$_{Se}$ crystal collected at the Se peak wavelength of 0.9794 Å. The program SHELXD[51] was used to identify 39 Se sites related by three-fold NCS, which were used to calculate phases and complete the heavy atom model in SHARP/autoSHARP[52]. Solvent flattening and NCS averaging in both SOLOMON[53] and DM[54] subsequently improved phases. Anisotropy was corrected in SHARP[52] to yield a set of phases and isotropic amplitudes, which were subsequently used in density improvement. The resulting electron density map allowed automatic building of an initial model using Buccaneer[54], which accounted for ~80% of the protein sequence. The model was manually completed and rebuilt with Coot[55] and O[56], using a three-fold symmetry-averaged map that was sharpened with a B factor of −100 $Å^2$. Tight three-fold NCS restraints were imposed throughout the refinement. Relaxation of these restraints did not result in a significant drop in R_{free}.

Refinement was initially done using BUSTER-TNT[57], followed at the final stages by alternating use of BUSTER-TNT[57] and phenix.refine[58]. Phenix.refine[58] with simulated annealing and TLS refinement with nine defined TLS groups gave an overall better result in model geometry as judged by MolProbity[59]. BUSTER-TNT[57] produced better guiding $F_o - F_c$ maps for model building, manifest in the improved overall refinement statistics. The final cycle of refinement was performed with BUSTER-TNT[57] (Supplementary Table 1). The model statistics resulting from MolProbity[59] are reported in Supplementary Table 1. The gap between R factors obtained during refinement for the working and test sets of reflections is surprisingly narrow. This is probably due to the strict NCS restraints used throughout the refinement and the test-set reflections being chosen randomly and not within small resolution shells.

Transport assay. Uptake of [^{14}C]glycine betaine mediated by BetP or BetPΔN29 was measured in *E. coli* MKH13, in *C. glutamicum* DHPF cells[21] and in *E. coli* polar lipid proteoliposomes as described[23]. The uptake rate was displayed relative to maximum. Absolute values are given in the legend of Supplementary Fig. 1. BetP mutants carrying the individual point mutations W194L, Y197L, W371L, W374L, W377L, P134AE135A, R210A, G301A, R387A and R392K were measured in *E. coli* MKH13[21] cells as described[23]. The BetP single point mutants W189C, W326C and W366C gave low expression yields in *E. coli* as judged by immunoblotting against the N-terminal StrepII tag and were therefore reconstituted into *E. coli* phospholipids[48] for transport measurements. The osmolality was adjusted to 800 mosmol kg^{-1} by addition of sorbitol. Substrate uptake in cells or proteoliposomes was initiated by adding [^{14}C]glycine betaine (0.1 mCi ml^{-1}) at a final concentration of 100 or 200 mM and measured as described[48].

49. Kabsch, W. Automatic processing of rotation diffraction data from crystals of initially unknown symmetry and cell constants. *J. Appl. Crystallogr.* **26,** 795–800 (1993).
50. Evans, P. Scaling and assessment of data quality. *Acta Crystallogr. D* **62,** 72–82 (2006).
51. Sheldrick, G. M. A short history of SHELX. *Acta Crystallogr. A* **64,** 112–122 (2008).
52. Vonrhein, C., Blanc, E., Roversi, P. & Bricogne, G. Automated structure solution with autoSHARP. *Methods Mol. Biol.* **364,** 215–230 (2007).
53. Abrahams, J. P. & Leslie, A. G. W. Methods used in the structure determination of bovine mitochondrial F_1 ATPase. *Acta Crystallogr. D* **52,** 30–42 (1996).
54. Cowtan, K. dm: An automated procedure for phase improvement by density modification. *CCP4/ESF-EACBM Newslett. Protein Crystallogr.* **31,** 34–38 (1994).
55. Emsley, P. & Cowtan, K. Coot: model-building tools for molecular graphics. *Acta Crystallogr. D* **60,** 2126–2132 (2004).
56. Jones, T. A., Zou, J.-Y., Cowan, S. W. & Kjeldgaard, M. Improved methods for the building of protein models in electron density maps and the location of errors in these models. *Acta Crystallogr. A* **47,** 110–119 (1991).
57. Blanc, E. *et al.* Refinement of severely incomplete structures with maximum likelihood in BUSTER-TNT. *Acta Crystallogr. D* **60,** 2210–2221 (2004).
58. Terwilliger, T. C. *et al.* Iterative model building, structure refinement and density modification with the PHENIX AutoBuild wizard. *Acta Crystallogr. D* **64,** 61–69 (2008).
59. Lovell, S. C. *et al.* Structure validation by C-alpha geometry: phi, psi, and C-beta deviation. *Proteins Struct. Funct. Genet.* **50,** 437–450 (2003).